ACADEMIA ROMÂNĂ
*Revue Roumaine de Chimie*
http://web.icf.ro/rrch/

*Rev. Roum. Chim.*,
**2016**, *61*(4-5), 337-344

*Dedicated to Professor Alexandru T. Balaban on the occasion of his 85th anniversary*

# SYNTHESIS AND STRUCTURAL CHARACTERIZATION OF STRONTIUM SUBSTITUTED HYDROXYAPATITES

Petre T. FRANGOPOL,[a] Aurora MOCANU,[a] Valer ALMASAN,[b] Corina GARBO,[a] Reka BALINT,[a] George BORODI,[b] Ioan BRATU,[b] Ossi HOROVITZ[a] and Maria TOMOAIA-COTISEL[a*]

[a] Babes-Bolyai University of Cluj-Napoca, Faculty of Chemistry and Chemical Engineering, Physical Chemistry Center, Chemical Engineering Department, 11 Arany J. Str., 400028 Cluj-Napoca, Roumania
[b] National Institute for Research and Development of Isotopic and Molecular Technologies, 65-103 Donath Str., 400293 Cluj-Napoca, Roumania

*Received December 21, 2015*

Novel strontium substituted nano hydroxyapatites of high crystallinity were prepared by a new wet chemical methodology, assisted by templates (ethylenediamine and o-toluidine), starting with calcium and strontium nitrates and diammonium hydrogen phosphate in stoichiometric ratio, processed in basic medium (ammonia). Urea-formaldehyde resin prepared *in situ* was also used to avoid the agglomeration of particles. After lyophilization, the organic matter was removed by calcination. Synthesized hydroxyapatites correspond to the formula $Ca_{10-x}Sr_x(PO_4)_6(OH)_2$ with x = 0 (pure hydroxyapatite, HAP), 0.59, 1.21 and 1.87 (HAP-Sr) as well as 10, corresponding to Ca totally substituted by Sr (SrHAP). They were characterized by XRD, FTIR and Raman spectroscopy, TEM and AFM. The analysis found strong correlations among Sr content, crystal size and crystallinity within nanopowders obtained. These nanomaterials revealed a controlled morphology and can be used in orthopedics as bone remodeling substitutes, and in dentistry, as anti-sensitizing agents and for re-mineralization of enamel.

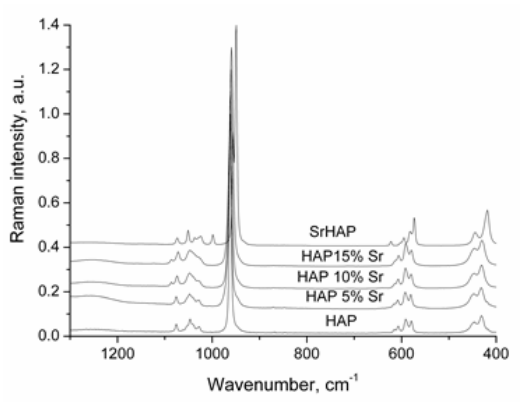


## INTRODUCTION

Hydroxyapatite (HAP) is well known as the main constituent of human bones, and there are great expectations regarding the use of synthetic HAPs in bone fracture treatment and bone replacement. The ideal chemical formula for HAP is $Ca_{10}(PO_4)_6(OH)_2$. HAP crystallizes in the hexagonal space group $P6_3/m$, with lattice parameters $a = b \neq c$; $\alpha = \beta = 90°$; $\gamma = 120°$. An important characteristic of HAP is that it allows for various isomorphic substitutions of $Ca^{2+}$ by other divalent cations, but also by monovalent or trivalent ones, while its anions $PO_4^{3-}$ and $OH^-$ can also be substituted by other anions, and thus, different stoichiometric or non-stoichiometric structures are possible. This opens a large way to improve physical, chemical and biological

* Corresponding author: mcotisel@chem.ubbcluj.ro; mcotisel@gmail.com

properties of hydroxyapatites (HAPs) in view of their biomedical applications.[1, 2]

Increasing attention is given recently to strontium substituted HAPs: $Ca_{10-x}Sr_x(PO_4)_6(OH)_2$, where x can vary continuously from 0 to 10 and to multi substituted hydroxyapatites, with $Sr^{2+}$ together with other cations ($Mg^{2+}$, $Zn^{2+}$, $Ce^{3+}$). The Sr substitution in HAP showed beneficial effects on bone formation and prevention of bone resorption,[3] for the treatment of osteoporosis,[4] since it promotes osteoblast proliferation and differentiation and reduces osteoclast activity.[5] Sr-substituted HAPs also present antimicrobial activity,[1,6] while their cell cytotoxicity is rather low.[7-9]

A great number of synthesis methods for HAPs substituted with Sr or with Sr and other elements, also named as ceramics and bone cements, were proposed. Solid state methods implied the preparation at high temperatures, by diffusion in the solid state.[10,11] Wet chemical methodologies include syntheses using concentrated initial solutions of reactants, as in sol-gel methods,[12-15] solution combustion synthesis,[16] and those using co-precipitation from more diluted solutions, with a subsequent thermal treatment to improve the crystallinity.[3,8,17-25] Mostly, $Ca(NO_3)_2$, $CaCl_2$ or $Ca(OH)_2$ were used as source for $Ca^{2+}$ ions, $Sr(NO_3)_2$ or $SrCl_2$ for $Sr^{2+}$, and $Na_2HPO_4$, $K_2HPO_4$, $(NH_4)_2HPO_4$ or $H_3PO_4$ for phosphate, with ammonia or NaOH to assure a basic medium. Sometimes, organic molecules such as amino acids (glycine), surfactants, inorganic compounds and various counterions are used as templates to control hydroxyapatite particle synthesis.[26, 27]

The goal of this work is to explore the influence of various templates in the synthesis methodology of nanoparticles of hydroxyapatites doped with Sr, which is contributing to the regeneration of bone. The focus is on the shape and size of nanoparticles and on the crystallinity and structure of resulted powders with applicability in hard tissue replacement and regeneration, as well as in enamel re-mineralization and drug delivery systems. Therefore, a new wet chemical methodology, mediated by templates (EDA and o-toluidine) coupled with urea-formaldehyde resin, has been developed and represents the first experimental design to synthesize nanostructured hydroxyapatite (HAP) and strontium substituted hydroxyapatites (HAP-Sr) until total substitution of Ca by Sr is reached (SrHAP). The obtained hydroxyapatites are further structurally and morphologically characterized by varied physico-chemical methods.

## RESULTS AND DISCUSSION

The syntheses were based on the reaction:

$$(10\text{-}x)Ca(NO_3)_2 + xSr(NO_3)_2 + 6(NH_4)_2HPO_4 + 8NH_4OH \rightarrow Ca_{10-x}Sr_x(PO_4)_6(OH)_2 + 20NH_4NO_3 + 6H_2O$$

where x has values from 0 to 10, as seen in Table 1 from theoretical formula. The strontium content, given in weight % and in the mol% of calcium substituted by strontium, is also shown in Table 1, for the substituted HAPs prepared by us.

**XRD patterns.** For the synthesized HAP and Sr-substituted HAP nanopowders, the XRD patterns were compared with the PDF (Powder Diffraction Files) for stoichiometric hydroxyapatite (HAP) and HAP-Sr compounds, respectively, as given in Table 2. The crystallite size was evaluated by the Scherrer method, from the width of the most intense diffraction peak, measured at half-maximum. The crystallinity degree of the samples was also estimated and the results are given in Table 2. Most of the diffraction peaks match well with those of the HAP and HAP-Sr compounds from the PDFs. There is no important modification caused by the incorporation of $Sr^{2+}$ ions as substituents for $Ca^{2+}$ ions in the HAP structure, and no supplementary peaks come out. There are only some variations in the intensity and the width of the peaks (broadening), probably due to lattice distortions by the inclusion of strontium. Although, the SrHAP sample (all Ca substituted by Sr), $Sr_{10}(PO_4)_6(OH)_2$, reveals a structure similar to that of hydroxyapatite, which is the major phase (Fig. 1a), the XRD patterns also indicate the presence of $Sr_3(PO_4)_2$, a compound crystallized in the rhombohedral system (Fig. 1b).

*Table 1*

Compositions of prepared strontium substituted hydroxyapatites

| Hydroxyapatites HAPs | Weight % Sr | Mol % Ca substituted by Sr* | Theoretical formula |
|---|---|---|---|
| HAP | 0 | 0 | $Ca_{10}(PO_4)_6(OH)_2$ |
| HAP-5%Sr | 5 | 5.9 | $Ca_{9.41}Sr_{0.59}(PO_4)_6(OH)_2$ |
| HAP-10%Sr | 10 | 12.1 | $Ca_{8.79}Sr_{1.21}(PO_4)_6(OH)_2$ |
| HAP-15%Sr | 15 | 18.7 | $Ca_{8.13}Sr_{1.87}(PO_4)_6(OH)_2$ |
| SrHAP | 59.2 | 100 | $Sr_{10}(PO_4)_6(OH)_2$ |

* $100\frac{n_{Sr}}{n_{Sr}+n_{Ca}}$

*Table 2*

XRD characterization of prepared HAP and strontium substituted hydroxyapatites

| Sample | Phases present (PDF number) | Crystal-linity degree, % | Crystals size, nm | Particles size from TEM, nm | Lattice parameters a=b; c [Å] | |
|---|---|---|---|---|---|---|
| | | | | | From PDF | Estimated, via Eqs. 1 and 2 |
| HAP | HAP (74-0566) | 78.5 | 59.9 | 61 ± 7 | 9.423; 6.883 | 9.424; 6.881 |
| HAP-5%Sr | HAP (74-0566) | 67.7 | 59.9 | 64 ± 10 | - - | 9.443; 6.903 |
| HAP-10%Sr | $Ca_9Sr(PO_4)_6(OH)_2$ (34-0484) | 77.1 | 75.7 | 76 ± 11 | 9.460; 6.920 | 9.463; 6.926 |
| HAP-15%Sr | $Ca_8Sr_2(PO_4)_6(OH)_2$ (34-0483) | 77.3 | 76.8 | 69 ± 13 | 9.486; 6.951 | 9.485; 6.951 |
| SrHAP | $Sr_{10}(PO_4)_6(OH)_2$ (12-0361) | 85.9 | 90.5 | 97 ± 16 | 9.745; 7.256 | 9.747; 7.255 |
| | $Sr_3(PO_4)_2$ (85-0902) (traces) | - | - | - | *a=7.295; $\alpha$=43.35$^0$ | - - |

* rhombohedral system

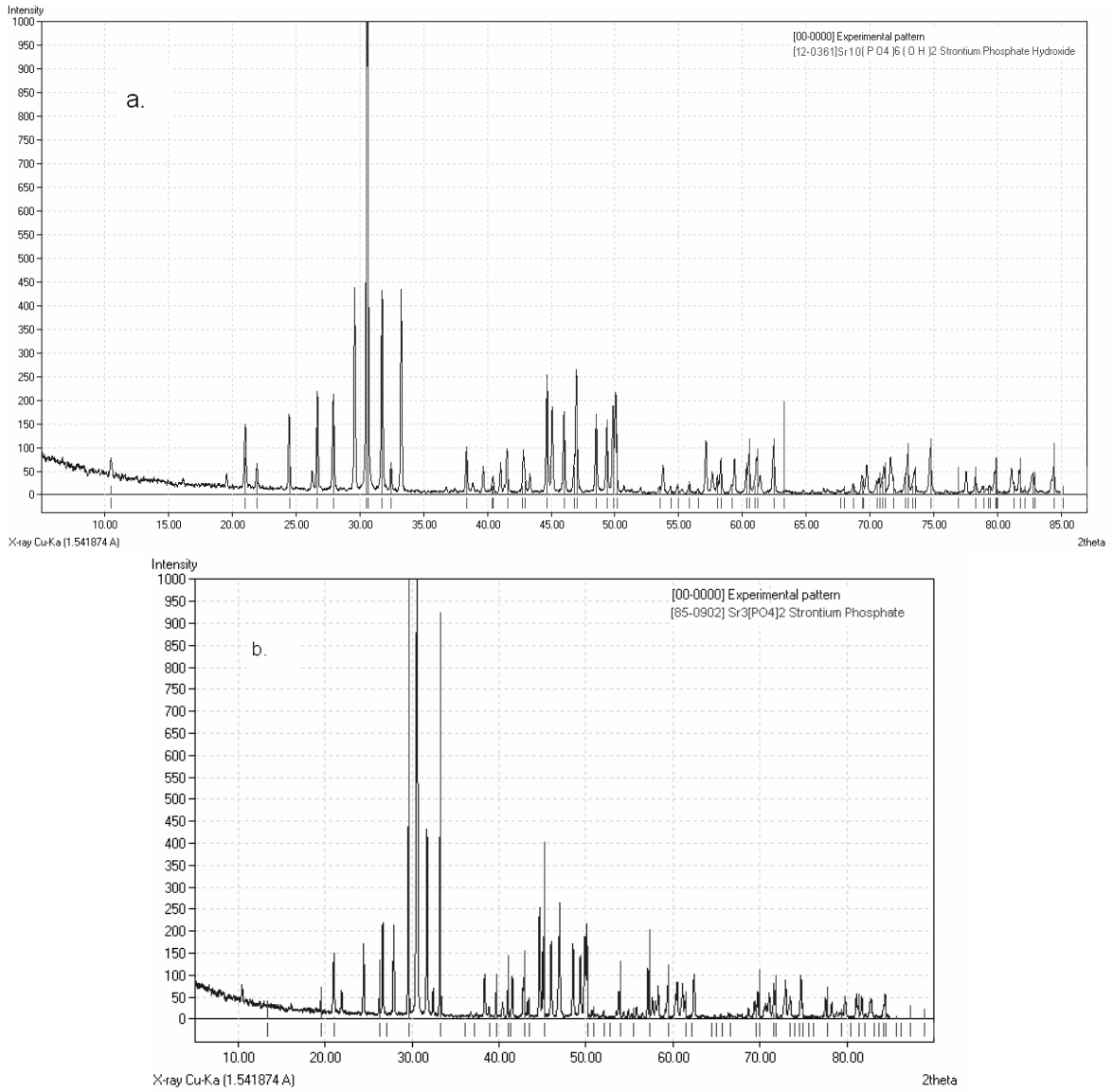


Fig. 1 – XRD pattern for the SrHAP nanopowder compared with PDF for $Sr_{10}(PO_4)_6(OH)_2$ (a) and for $Sr_3(PO_4)_2$ (b).

The XRD investigations confirm that the strontium substituted hydroxyapatites maintained the same hydroxyapatite crystalline structure (hexagonal system, space group $P6_3/m$) as stoichiometric HAP. The values of the lattice parameters a and b increase with increasing Sr content, due to the higher ionic radius of $Sr^{2+}$ (112 pm) as compared with that for $Ca^{2+}$ (100 pm).[28] As a result, a shift in the position of diffraction peaks toward lower 2θ values is observed.[22] Further, a deep analysis revealed a clear linear correlation between lattice parameters and the Sr-index x in the formula of the Sr-substituted HAPs, described by the following equations:

$$a = b\ [Å] = (9.4243 \pm 0.0021) + (0.0323 \pm 1.6 \cdot 10^{-4})x \qquad r^2 = 0.9997 \qquad (1)$$

$$c\ [Å] = (6.8808 \pm 0.0025) + (0.0374 \pm 1.7 \cdot 10^{-4})x \qquad r^2 = 0.9997 \qquad (2)$$

Using these relations, we found the lattice parameters (a = b; c), which are given in the last column of Table 2, for the all prepared HAPs.

The crystallinity degree of the nanostructured samples is rather high (70-80%). As expected,[21] it is the highest for pure HAP and SrHAP, and the lowest for low Sr content (HAP-5%Sr), as a consequence of the difficulty for the first larger $Sr^{2+}$ ions to be accommodated in the lattice of pure calcium hydroxyapatite.

**FTIR spectra** of HAP and of substituted hydroxyapatites are compared in Fig. 2a. The spectra in Fig. 2 are normalized to the most intense $\nu_3$ band and their ordinates are shifted on the vertical axes for comparison. The absorption bands can be assigned to vibrations due to the phosphate group and to the structural OH group of HAPs as well as to absorbed water.

The vibrations of the P-O bonds within the $PO_4$ groups appear in the 1100-450 $cm^{-1}$ region. The symmetric P-O stretching mode $\nu_1$ should be inactive in IR for an ideal tetrahedral symmetry ($T_d$) of the $PO_4$ group.[29] Nevertheless, it appears with a low intensity in the FTIR spectra, at 962-949 $cm^{-1}$, as a result of the lowering of symmetry due to the deformation of the tetrahedron in these phosphates as against the free $PO_4^{3-}$ ions.[30] The strongest IR absorption band corresponds to the asymmetric P-O stretching mode $\nu_3$. This band is triply degenerate in the free phosphate ions.[29] Thus, at lower symmetry it can be split into three separate modes. In the spectra the main maximum appears at wavenumbers from 1046 (HAP) to 1031 $cm^{-1}$ (SrHAP), and another maximum appears at 1091-1076 $cm^{-1}$. Absorptions due to the bending modes in the $PO_4$ group appear at lower wavenumbers. The bands in the 600-560 $cm^{-1}$ region can be assigned to the asymmetric P-O bending $\nu_4$. It is again a triply degenerate mode for $T_d$ symmetry, but it is split into at least two components in hydroxyapatite.[31] In our spectra two defined peaks are observed in this region. The lowest frequency absorption band, at 474-456 $cm^{-1}$, is assigned to the symmetric bending mode, $\nu_2$. For all the absorption bands of the $PO_4$ group, the values of the wavenumbers decrease with increasing strontium content, in accordance with the observations of Bigi *et al.*,[21] but are constant from 0 to 15 wt% Sr, as observed by Terra *et al.*[24] An explanation is based on the larger ionic radius of $Sr^{2+}$ against $Ca^{2+}$, which determines increasing distances between the phosphate anions, and subsequently, lower repulsion forces among them.[21,32]

Absorption bands due to H-O vibrations include the broad band at 3600-3300 $cm^{-1}$ of absorbed water with hydrogen bonding O-H…O in the samples, while the band due to H-O-H bending has the maximum at about 1630 $cm^{-1}$. Their position does not change with the Sr content. The first band overlaps with the narrow band of structural OH (from hydroxyapatite)[33, 34] at 3572 $cm^{-1}$, but at 3591 $cm^{-1}$ in SrHAP. A band due also to structural OH (libration vibration) is observed at 633 $cm^{-1}$. The intensities of these two bands slightly decrease with increasing Sr content in the samples, as previously observed by Terra *et al.*,[24] for similar compounds.

The same shift of $PO_4$ absorption bands with increasing Sr content is observed in the *Raman spectra* (Fig. 2b). Here the symmetric P-O stretching mode $\nu_1$, forbidden in IR, gives the most intense signal. Its wave number is shifted from 961 $cm^{-1}$ for HAP to 948 $cm^{-1}$ for SrHAP.

**TEM images** for HAP with 15 wt% Sr are given as example in Fig. 3, along with the histogram of size distributions for the HAP-Sr particles. The histogram was obtained by measuring the diameters of a large number of particles (hundreds) from multiple images for the same HAP- 15 wt% Sr sample. The mean value and the corresponding error are given for each sample in Table 2. The particles have irregular shapes and show a tendency to group together in

large swarms. For all synthesized materials, the size of particles is within nano scale.

An example of **AFM images** for HAP with 5 wt% Sr is given in Fig. 4. The size of particles, as viewed on the AFM images, are comparable with those obtained by TEM and RXD investigations.

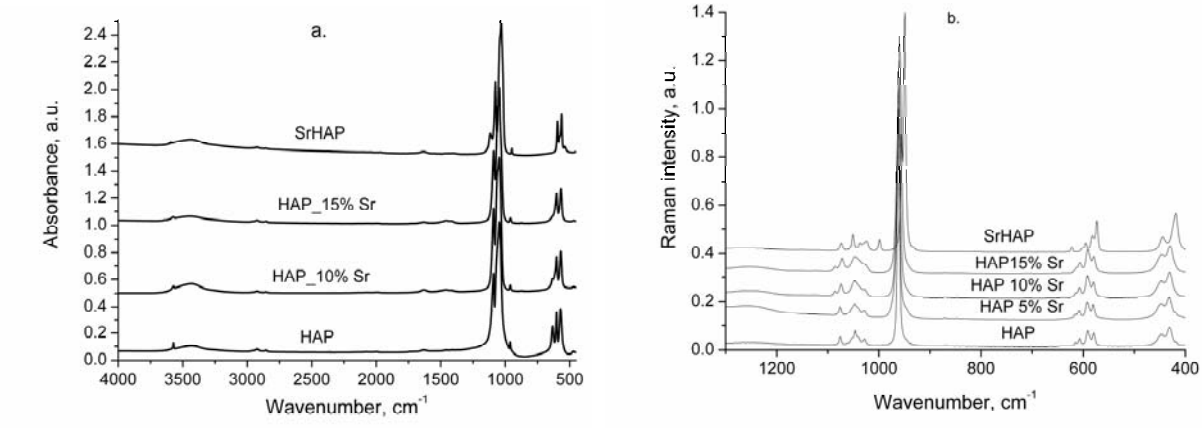


Fig. 2 – Normalized FTIR spectra (a) and Raman spectra (b) of HAP and Sr-substituted HAPs.

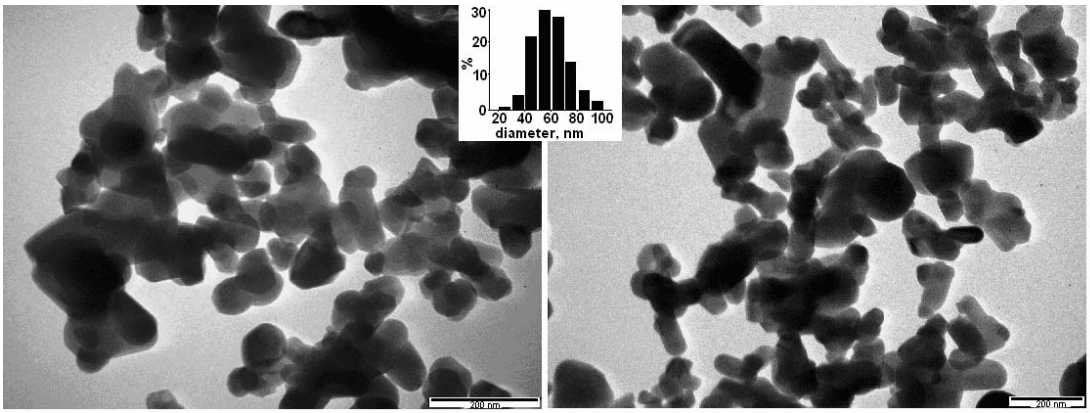


Fig. 3 – TEM images for HAP-15% Sr and histogram of size distribution; bars length: 200 nm; average diameter of the particles: $\overline{d}$ = 69 ± 13 nm.

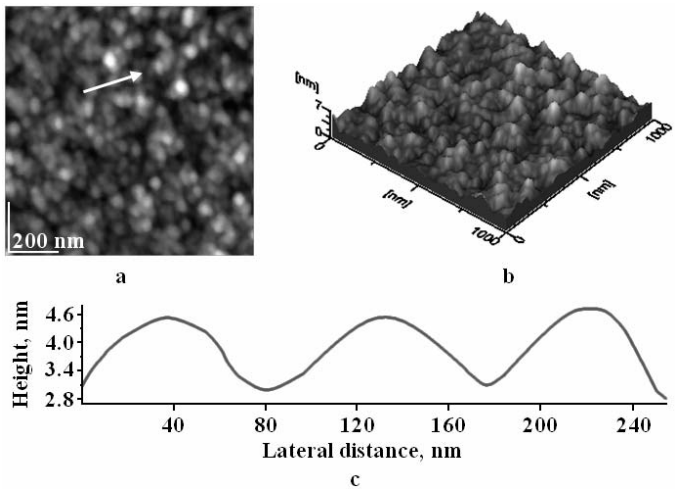


Fig. 4 – HAP-5%Sr adsorbed on glass for 30 s from aqueous dispersion: (a) 2D-topographic image; (b) 3D-topographic image; (c) cross section profile along the arrow in panel (a); scanned area: 1 μm x 1 μm; average particle size 62 ± 5 nm.

**Zeta potential** measurements on sample powders dispersed in water gave slightly negative values for HAP (-13.6 mV), as well as for substituted HAP comprising 10 wt% Sr (-16.7 mV) and for SrHAP (-18.1 mV). The negative charge is probably due to the preferential adsorption of $HO^-$ ions from the aqueous medium.

## EXPERIMENTAL

**Materials.** Calcium nitrate tetrahydrate, $Ca(NO_3)_2 \cdot 4H_2O$ (POCH S.A., Poland) and strontium nitrate, $Sr(NO_3)_2$ (CHEMPUR, Poland) were used together with diammonium hydrogen phosphate, $(NH_4)_2HPO_4$ (S.C Nordic Invest SRL, Romania), as raw materials. Ethylenediamine, EDA (Sigma-Aldrich, Switzerland) and o-toluidine (Merck) were used as templates. Urea was obtained from Honeywell (USA), and formaldehyde and ammonia solutions from CHEMPUR (Poland). All chemicals used were of analytical grade or of the highest purity available. They were used as received without further purification. Aqueous solutions were prepared with double distilled water, further deionized (resistivity of 18 Mohm·cm) in Elgastat water purification system.

**Preparation of hydroxyapatites:** In order to obtain nanostructured pure hydroxyapatite and strontium substituted hydroxyapatites, the general procedure, previously developed by us, [2, 35-39] was further improved, to give a novel template-mediated precipitation methodology. Briefly, two solutions were prepared. **Solution 1** comprises the 0.25 M ($Ca^{2+}$, $Sr^{2+}$, or $Ca^{2+}$ + $Sr^{2+}$) solution, prepared by dissolving the calculated amounts of $Ca(NO_3)_2 \cdot 4H_2O$ and/or $Sr(NO_3)_2$ in ultrapure water, to which o-toluidine was added to about 8% of the final product mass. Further, 25% ammonia solution was added, to assure a pH value of 8.5. **Solution 2** comprises the 0.15 M $PO_4^{3-}$ solution, which was obtained by dissolving $(NH_4)_2HPO_4$ in ultrapure water. To this solution, o-toluidine and EDA were added, each of them at about 8% of the final product mass. Lastly, the pH value was fixed at 11.5 by adding 25% ammonia solution. The templates were added in order to monitor the crystallite growth within the nanometric scale, by their adsorption on the surface of the developing solid phase.

A quite strong mixing, for milliseconds, of the two solutions was assured using a peristaltic pump Masterflex L/S Digital Drive, 600 RPM, 115/230 VAC, EW-07523-80, and an impact reactor type "Y" for the two liquid flows containing the reactants in stoichiometric molar ratio, $(Ca^{2+} + Sr^{2+})/PO_4^{3-} = 5/3$. The reactants were mixed at room temperature and a suspension was instantaneously obtained. To achieve the specific hydroxyapatite structure, a maturation process was allowed for the obtained suspension, by maintaining it at a temperature of 80-90°C, for at least 10 h, as the average time required for its maturation.

The agglutination or forming of conglomerates during the subsequent operations (e.g., filtering, washing, drying) was avoided by adding urea formaldehyde resin, to surround the surface of each HAP particle in matured aqueous dispersion. The resin represented about 10% of the final product mass and was prepared *in situ*, by adding 37% aqueous formaldehyde solution and urea for the molar formaldehyde/urea ratio, in the range of 1.1-1.3, with a final pH value of 8.2-8.5. The so obtained precipitate was filtered and washed with ultrapure water, until free of nitrate anions. After lyophilization, the solid product obtained was disintegrated in a ball mill, for 2 h. The obtained samples were calcined in air, in two steps, namely at temperatures of 550ºC for 6 h and at 850ºC for 4h, to burn the organic matter and to increase the crystallinity of the final product. The significant influence of the preparation methodology on the structure of the respective products is evidenced in this work for various hydroxyapatites, and it is also documented for the fabrication of various other compounds. [40-42]

**Characterization methods**

**X-Ray Diffraction** (XRD) investigations were carried out using a Bruker D8 Advance diffractometer, in Bragg-Brentano geometry, equipped with a X-ray tube with copper $K_\alpha$ line, wavelength 1.541874 Å), a Ge (111) monochromator and an EyeLynx position detector.

**FTIR spectra** were recorded by the KBr pellets method, with a spectrometer JASCO 6100 in the 4000-400 $cm^{-1}$ range of wave numbers, with a 2 $cm^{-1}$ resolution. **Raman FT spectra** were obtained with a FRA 106/S FT-Raman Module attached to Bruker EQUINOX 55; an Nd:YAG laser was used (wavelength 1064 nm) and a liquid nitrogen cooled germanium detector (D418-T).

The samples were investigated with a **transmission electron microscope** (TEM, JEOL – JEM 1010). The particles were adsorbed from their aqueous dispersions on the specimen grids. Then, the samples were air dried. TEM images[43, 44] were recorded with JEOL standard software. **Atomic force microscopy**, AFM, imaging was obtained using the AFM JEOL 4210 equipment, operated in tapping mode,[45-47] using standard cantilevers with silicon nitride tips (resonant frequency in the range of 200-300 kHz, spring constant 17.5 N/m). The particles were adsorbed from their aqueous dispersion for 10 or 30 s, on solid support (glass). Different areas from 10 μm x 10 μm to 0.5 μm x 0.5 μm were scanned on the same film. The AFM images (2D- and 3D-topographies) and the cross-section profile in the film, along a selected direction, were processed by the standard procedures.

**Zeta potential** measurements were performed, using the Malvern Zetasizer Nano-ZS90, on aqueous dispersions of the obtained nanopowders.

## CONCLUSIONS

A new aqueous precipitation methodology, assisted by templates (EDA and o-toluidine) coupled with urea-formaldehyde resin, has been developed to synthesize pure HAP and Sr substituted HAPs with variable Sr content (HAP-Sr), up to 100 mol% substitution of Ca by Sr (SrHAP). This experimental design makes possible the preparation of monophasic HAP and HAP-Sr nanomaterials, with the lattice structure characteristic for pure stoichiometric HAP, as revealed by XRD investigations. FTIR and Raman spectra confirmed this HAP structure, in all synthesized Sr substituted HAP samples. TEM and AFM imaging evidenced the average particle size in the nanometric domain for all synthesized nanomaterials. Overall, these results on the size of crystallites and the degree of crystallinity for HAPs

in conjunction with our previous reported data[2, 35-39] show a remarkable influence of the preparation technique on the respective structures. Thus, the template mediated wet chemical methodology, reported here, leads to highly crystalline products with controlled nano structure and morphological features. The biological investigations are in progress in our laboratories, in order to assess the biocompatibility of these new HAP-Sr nanomaterials, for potential applications in biomedical engineering, especially in orthopedic, dental and maxillofacial field.

*Acknowledgements:* We acknowledge the Executive Agency for Higher Education, Research, Development and Innovation Funding (UEFISCDI) for financial support through the scientific research projects no. 171 and 241.

## REFERENCES

1. D. Gopi, S. Ramya, D. Rajeswari, P. Karthikeyan and L. Kavitha, *Coll. Surf. A*, **2014**, *451*, 172–180.
2. A. Mocanu, G. Furtos, S. Răpuntean, O. Horovitz, C. Flore, C. Garbo, A. Dănişteanu, G. Răpuntean, C. Prejmerean and M. Tomoaia-Cotisel, *Appl. Surf. Sci.*, **2014**, *298*, 225-235.
3. H.B. Pan, Z.Y. Li, W.M. Lam, J.C. Wong, B.W. Darvell, K.D.K. Luk and W.W. Lu, *Acta Biomater.*, **2009**, *5*, 1678-1685.
4. G.X. Ni, W.W. Lu, B. Xu, K.Y. Chiu, C. Yang, Z.Y. Li, W.M. Lam and K.D.K. Luk, *Biomaterials*, **2006**, *27*, 5127–5133.
5. A.R. Boyd, L. Rutledge, L.D. Randolph and B.J. Meenan, *Mater. Sci. Eng. C,* **2015**, *46*, 290–300.
6. N. D. Ravi, R. Balu and T.S. Sampath Kumar, *J. Amer. Ceramic Soc.*, **2012**, *95*, 2700-2708.
7. Z.H. Li, J.M. Wu, S.J. Huang, J. Guan and X.Z. Zhang, *Adv. Mater. Res.*, **2011**, *160-162*, 117-122.
8. D. dos Santos Tavares, C.X. Resende, M.P. Quitan, L. de Oliveira Castro, J.M. Granjeiro and G. de Almeida Soares, *Mater. Res.*, **2011**, *14,* 456-460.
9. Y.F. Fu, D.M. Chen and J.Z. Zhang, *Shanghai Kou Qiang Yi Xue*. **2002,** *11(3),* 229-232. PMid:14983257.
10. A. Bigi, G. Falini, M. Gazzano, N. Roveri and E. Tedesco, *Mater. Sci. Forum*, **1998**, *278-281*, 814-819.
11. F.E. Imrie, V. Aina, G. Lusvardi, G. Malavasi, I.R. Gibson, G. Cerrato and B. Annaz, *Key Eng. Mater.*, **2013**, *529-530*, 88-93.
12. Y. Lin, Z. Yang, J. Cheng and L. Wang, *J. Wuhan Univ.Technol.–Mater. Sci. Ed.*, **2008**, *23*, 475-479.
13. A. Balamurugan, G. Balossier, P. Torres, J. Michel and J.M.F. Ferreira, *Mater. Sci. Eng* .C, **2009,** *29*, 1006-1009.
14. C.M. Mardziah, I. Sopyan and S. Ramesh, *Trends Biomater. Artif. Organs*, **2009**, *23*, 105-113.
15. H. Paennarin and S.L. Seet, *Chiang Mai J. Sci.*, **2013,** *40*, 1055-1060.
16. M. Kavitha, R. Subramanian, R. Narayanan and V. Udhayabanu, *Powder Technol*., **2014**, *253*, 129–137.
17. R. L. Collins, *J. Amer. Chem. Soc.***1959**, *81*, 5275-5278.
18. J. Sun, M. Xue, M. Kikuchi, M. Akao and H. Aoki, *Biomed. Mater. Eng*., **1994**, *4*, 503–512.
19. S.C. Verberckmoes, G.J. Behets, L. Oste, A.R. Bervoets, L.V. Lamberts, M. Drakopoulos, A. Somogyi, P. Cool, W. Dorrine, M.E. De Broe and P.C. D'Haese, *Calcif. Tissue Int*., **2004**, *75*, 405–415.
20 Z.Y. Li, W.M. Lam, C. Yang, B. Xu, G.X. Ni, S.A. Abbah, K.M.C Cheung, K.D.K. Luk and W.W. Lu, *Biomaterials*, **2007**, *28*, 1452-1460.
21. A. Bigi, E. Boanini, C. Capuccini and M. Gazzano, *Inorg. Chim. Acta*, **2007**, *360*, 1009-1016.
22. M.D. O'Donnell, Y. Fredholm, A. de Rouffignac and R.G. Hill, *Acta Biomater.*, **2008**, *4*, 1455–1464.
23. C. Capuccini, P. Torricelli, F. Sima, E. Boanini, C. Ristoscu, B. Bracci, G. Socol, M. Fini, I.N. Mihailescu and A. Bigi, *Acta Biomater.*, **2008**, *4*, 1885–1893.
24. J. Terra, E.R. Dourado, J.G. Eon, D.E. Ellis, G. Gonzalez and A. M. Rossi, *Phys. Chem. Chem. Phys.*, **2009**, *11*, 568-577.
25. I. Abdullahi and S.A. Thomas, *Nigerian J. Basic Appl. Sci.*, **2009**, *17*, 177-180.
26. W. Xia, K. Lin, Z. Gou and H. Enqvist, In "Hydroxyapatite: Synthesis, Properties and Application", V. S. Gshalaev and A. C. Demirchan, Eds., Nova Science Publ., New York, 2012, p. 243-264.
27. D. Gopi, S. Nithiya, L. Kavitha and J. M.F. Ferreira, *Bull. Mater. Sci*., **2012**, *35*, 1195–1199.
28. E. Bryan and L. D. R. Wilford, "Chemistry Data Book", Nelson Thornes Ltd, Cheltenham, UK, 1992.
29. V.M. Bhatnagar, *Experientia*, **1967**, *23*, 10-12.
30. W.E. Klee and G. Engel, *J. Inorg. Nucl. Chem.*, **1970**, *32*, 1837-1843.
31. C.B. Baddiel and E.E.Berry, *Spectrochim. Acta*, **1966**, *22*, 1407-1416.
32. B.O. Fowler, *Inorg. Chem.*, **1974**, *13*, 194-207; 207-214
33. K. Nakata, T. Kubo, C. Numako, T. Onoki and A. Nakahira, *Mater. Trans*., **2009**, *50*, 1046-1049.
34. A.Y. Pataquiva-Mateus, C.C. Barrias, C. Ribeiro, M.P. Ferraz and F.J. Monteiro, *J. Biomed. Mater. Res.*, A, **2008**, *86*, 483-493.
35. G. Tomoaia, O. Soritau, M. Tomoaia-Cotisel, L.-B. Pop, A. Pop, A. Mocanu, O. Horovitz and L.-D. Bobos, *Powder Technol.*, **2013,** *238*, 99-107.
36. G. Tomoaia, A. Mocanu, I. Vida-Simiti, N. Jumate, L. D. Bobos, O. Soritau and M. Tomoaia-Cotisel, *Mater. Sci. Eng. C*, **2014**, *37*, 37-47.
37. C. Garbo, M. Sindilaru, A. Carlea, G. Tomoaia, V. Almasan, I. Petean, A. Mocanu, O. Horovitz and M. Tomoaia-Cotisel, *Particul. Sci. Technol.*, **2015**, DOI: 10.1080/02726351.2015.1121180.
38. G. Tomoaia, M. Tomoaia-Cotisel, L. B. Pop, A. Pop, O. Horovitz, A. Mocanu, N. Jumate and L.D. Bobos, *Rev. Roum. Chim.,* **2011**, *56*, 1039-1046.
39. G. Tomoaia, L. B. Pop, I. Petean and M. Tomoaia-Cotisel, *Mater. Plast*., **2012**, *49*, 48-54.
40. L. Bogatu and R. Dragomir, *Rev. Chim.(Bucharest),* **2015**, *66*, 722-726.
41. L. Bogatu, *Rev. Chim. (Bucharest),* **2014**, *65*, 1230-1234.

42. V. Dinoiu, D. Florescu and L. Bogatu, *Rev. Chim. (Bucharest),* **2007**, *58*, 183-185.
43. G. Tomoaia, O. Horovitz, A. Mocanu, A. Nita, A. Avram, Cs. P. Racz, O. Soritau, M. Cenariu and M. Tomoaia-Cotisel, *Coll. Sur. B*, **2015**, *135*, 726-734.
44. A. Mocanu, R. D. Pasca, G. Tomoaia, C. Garbo, P.T. Frangopol, O. Horovitz and M. Tomoaia-Cotisel, *Int. J. Nanomedicine*, **2013**, *8*, 3867-3874.
45. O. Horovitz, G. Tomoaia, A. Mocanu, T. Yupsanis and M. Tomoaia-Cotisel, *Gold Bull.*, **2007**, *40*, 295-304.
46. M. Tomoaia-Cotisel, A. Tomoaia-Cotisel, T. Yupsanis, G. Tomoaia, I. Balea, A. Mocanu and Cs. Racz, *Rev. Roum. Chim.,* **2006**, *51*, 1181-1185.
47. P.T. Frangopol, D.A. Cadenhead, G. Tomoaia, A. Mocanu and M. Tomoaia-Cotisel, *Rev.Roum. Chim.,* **2015**, *60*, 265-273.